CHAPTER VII

ELECTROLYTIC ADMICELLAR POLYMERIZATION OF PYRROLE ON NATURAL RUBBER/CLAY NANOCOMPOSITES

7.1 Abstract

Organic–inorganic composites consisting of natural rubber (NR), polypyrrole (PPy), and sodium montmorillonite (Na-MMT) were synthesized via electrolytic admicellar polymerization. A constant potential of 9 volts was chosen for the synthesis. The PPy concentration was fixed at 100 mM, and the clay contents were varied from 1 to 7 parts per hundred of rubber (phr). The synthesized nanocomposites were characterized by Fourier transform infrared spectroscopy (FTIR), X-ray diffraction (XRD), scanning electron microscopy (SEM), and transmission electron microscopy (TEM), together with thermal stability (TGA), mechanical properties, and electrical conductivity (σ_{dc}) studies. The FTIR spectra indicated the characteristic peaks of both PPy and MMT clay and also evidenced a slight interaction between the PPy chain and the clay layers, verifying the success of electrolytic admicellar polymerization. XRD and TEM results pointed out the good dispersion of clay platelets in the polymer matrix, suggesting an exfoliated structure. The morphology of the nanocomposites was greatly dependent on the amount of MMT clay, especially at a 7 phr loading. The initial modulus and tensile strength of the nanocomposites containing the 7 phr loading were about 4 and 2 times higher, compared to unfilled NR/PPy, respectively. Thermal stability studies revealed a slight improvement in the decomposition temperature for the PPy component by the clay layers, while the opposite trend was found for the NR component. More interestingly, the electrical conductivity of the admicelled rubber increased significantly (~19–32 times) with increasing clay contents from 1 to 7 phr, in comparison with unfilled NR/PPy.

Keywords: Core–Shell Polymer; Nanocomposites; Polypyrrole; Natural Rubber; Clay

7.2 Introduction

Electrically conducting polymers have attracted a great deal of interest owing to their excellent conductivity and electrical applications [1, 2]. Among them, polypyrrole (PPy) is one of the most promising materials because of its ease of synthesis, good electrical conductivity, and environmental stability [3]. Normally, PPy can be synthesized via chemical oxidative and electrochemical polymerizations. The latter provides a better control of the film thickness, morphology, and better conductivity compared to the former method [4, 5]. However, poor processability, brittleness, and insolubility are limitations of PPy [3].

As we know, organic–inorganic hybrid nanocomposites provide superior performance in terms of mechanical properties, thermal stability, gas barrier, flame retardance, etc., when compared to individual organic polymers or conventional filled composites [3, 6]. Among the many clay minerals, sodium montmorillonite (Na-MMT) has been extensively adapted for the preparation of nanocomposites by means of its ability to undergo cation exchange with other organic or inorganic cations and to separate them into individual layers (about 1 nm) with a very high aspect ratio (high length-to-width ratio). Depending on the state of dispersion of the layered silicates, nanocomposites can be classified into either intercalated or exfoliated structures. Generally, an exfoliated structure is required, owing to the excellent reinforcing efficiency of fully delaminated layered silicates. There are numerous studies reporting on the preparation and evaluation of PPy-based nanocomposites. Liu et al. [5] prepared PPy/MMT nanocomposites via an electropolymerization technique on a gold substrate. The resulting composites showed an improvement in thermal stability, and also in electrical conductivity, from 26.4 to 634 Scm^{-1} (~ 24 times). Meanwhile, PPy/MMT nanocomposites, prepared by an inverted emulsion pathway polymerization method [3, 6] using dodecylbenzenesulfonic acid (DBSA) as both an emulsifier and a dopant, and ammonium persulfate (APS) as an oxidant, showed the opposite trend. The existence of the layered silicates weakened the interchain interaction of PPy and interrupted the delocalization of electrons, resulting in a decrease in electrical conductivity from 20 Scm^{-1} of unfilled PPy to 6 Scm^{-1} of PPy/MMT nanocomposites. Ray et al. [7]

prepared PPy/MMT nanocomposites through the chemical polymerization of pyrrole with MMT and $FeCl_3$-impregnated MMT in bulk and in aqueous medium. The synthesized composites showed a bulk conductivity in the range of 1.3×10^{-5} to 26×10^{-5} Scm^{-1}, depending on the level of $FeCl_3$ impregnation and content of PPy.

With regards to the presence of a core–shell structure, Lascelles et al. [8] synthesized PPy-coated micrometer-sized poly(N-vinylpyrrolidone)-stabilized polystyrene (PS) latexes via the in situ deposition of the conducting polymer from aqueous solution. The morphology, colloidal stability, and electrical conductivity of the coated latexes strongly depended on PPy loading. At high PPy content, both the original sizes of the PS particles and the submicron-sized PPy were formed as a separate sub-phase, thus causing a high electrical conductivity (2–6 Scm^{-1}) but poor colloid stability, whereas a smooth and uniform coating of globular PPy overlayer on PS particles, providing good colloid stability of the coated latexes, was found at a lower content of PPy (less than 10%). Bunsomsit et al. [9] reported the formation of PPy ultrathin films on NR latex particles ("core–shell structure") via admicellar polymerization, which is a technique using physically adsorbing surfactants as a reaction template. According to that work, in the presence of salt, the surfactant adsorption and pyrrole adsolubilization were improved, resulting in a smooth and homogeneous coating of PPy onto the latex surface, together with higher electrical conductivity (1.45×10^{-6} Scm^{-1}) than PPy-coated latex prepared without salt (0.96×10^{-6} Scm^{-1}). However, the electrical conductivity of PPy-coated latex prepared with/without salt showed a high improvement compared to that of pure NR (10^{-15} Scm^{-1}). Another work, by Genetti et al. [10], showed that through admicellar polymerization, nickel flakes were successfully coated with PPy. Additionally, its composite with polyethylene (LDPE) also exhibited an improvement in electrical conductivity by three orders of magnitude, compared with the neat nickel-filled LDPE. Recently, Chirasakulkarun et al. [11] reported the success of admicellar polymerization of PPy-coated NR latex particles using the electrochemical method. The authors also investigated the influence of applied voltages and monomer concentrations on the polymerization. It was found that the polymerization time was decreased with an increase in voltage from 6 to 15 volts; however, a voltage higher than 9 volts showed the corrosion effect on the copper electrodes, especially at 15

volts. For the monomer contents, as the pyrrole content increased from 20 to 800 mM, faster polymerization, a smoother surface coating, a higher thermal decomposition temperature, and higher electrical conductivity were achieved. Therefore, in this study, electropolymerization is carried out at an applied voltage of 9 volts and a monomer concentration of 100 mM, which is a concentration well beyond the percolation threshold for the PPy-coated NR latexes. To our knowledge, the formation of an ultrathin conducting polymer (PPy) on electrically insulating substrates can overcome the poor processability of PPy and improve the electrical conductivity of insulating substrates. When considering flexible and elastic substrates like NR, the obtained composites can be used as flexible smart materials which may find applications in electromagnetic interference shielding (EMI), microwave absorbents, static charge dissipating films, mechanical actuators (strain sensor), and wearable devices for fitting and training, etc. [12, 13]

In this present article, we explore the first exfoliated nanocomposites of conducting polymer (PPy), NR, and layered silicates (Na-MMT), which are successfully synthesized via electrolytic admicellar polymerization. The obtained nanocomposites are characterized by Fourier transform infrared spectroscopy (FTIR) for determining the success of the electrolytic admicellar polymerization. X-ray diffraction (XRD), scanning electron microscopy (SEM), and transmission electron microscopy (TEM) investigations are carried out for characterizing the dispersion of the layered silicates and the morphology of the nanocomposites, respectively. Finally, the unique and interesting results in thermal stability, mechanical properties, and electrical conductivity of the composites are reported.

7.3 Experimental Parts

7.3.1 Materials

Natural rubber latex, with 60% dry rubber content, was kindly provided by Rubber Research Institute (Thailand). Pyrrole monomer, with 97% purity (Aldrich), was stored in a refrigerator at 4°C prior to use. Dodecyl sulfate sodium salt (SDS) was purchased from Aldrich Chemical Company and was used without further purification. Pristine sodium montmorillonite (Na-MMT), with a

cation exchange capacity (CEC) of 115 meq/100g and a particle size of 325 meshes (< 45 μm), was kindly supplied by Kunimine Industries Co., Ltd., Tokyo, Japan, and was used as received.

7.3.2 Electrolytic Admicellar Polymerization

7.3.2.1 Admicelle Formation

In a typical experiment, 25 g of centrifuged NR latex was dispersed in distilled water in a reaction vessel containing a magnetic stirring bar. Then, a 1 wt% clay aqueous suspension was poured into the solution to achieve the clay contents of 1, 3, 5, and 7 parts per hundred of rubber (phr) with continuous stirring for 24 hr (the total volume of distilled water was 500 ml); after that 2.31 g of anionic surfactant (SDS) was added to the system while stirring for 2 hr before adjusting the pH. Normally, the point of zero charge (PZC) of NR is 3.9 at room temperature [9]. To obtain the admicelle formation, hydrochloric acid (HCl) was used to adjust the pH of the system to below the PZC of NR (normally adjusted to 3.0). After that, the mixture was once again stirred for another 24 hr. Nevertheless, it should be mentioned here that HCl was also used as a dopant for this electrolytic admicellar polymerization.

7.3.2.2 Monomer Adsolubilization and Electrochemical Polymerization

Under continuous stirring for 1 hr to ensure the monomer adsolubilization, 3.46 ml of pyrrole monomer was added to the mixture. Then, the electrochemical polymerization was performed at a constant potential of 9 V (at room temperature) using copper plates (2 cm × 10 cm) as both cathode and anode electrodes. As a consequence, dark NR/PPy/MMT nanocomposites having contents of 78.2–84.5/14.3–15.5/0–7.5 wt%, respectively, were synthesized and deposited at the anode electrode. To study the dispersion of clay layers, some of the solution was collected for transmission electron microscopy (TEM). It is noteworthy that the pH was maintained at 3.0 during the electrochemical polymerization, and both electrodes were changed every 2 hr to prevent the copper sheets from being corroded. Finally, the polymerization time was recorded from the beginning of the application of

constant potential until nothing was found on the anode electrode. After the polymerization had ended, the separated composites were collected on a Buchner funnel and washed with distilled water twice to remove the surfactant. The synthesized nanocomposites were dried in a vacuum oven at 70°C overnight and were further molded into 3 mm thick sheets, for performing the characterizations, using a hydraulically operated press at 160°C for 15 min.

As a comparison, the control sample was synthesized by using the same preparation method as mentioned before, without adding any pristine clay into the system. For the sample code, NR/PPy stands for the control sample, and NR/PPy/x-MMT stands for the nanocomposites, in which x indicates the weight of pristine clay per hundred of rubber (phr).

7.3.3 Characterizations

The structure of the composite films was investigated using a horizontal attenuated total reflection-Fourier transform infrared spectrometer (Nexus 670, HATR module) in the absorption mode. The spectra were recorded over a frequency range of 600–4000 cm^{-1} using air as a background.

Elemental analysis of the pristine clay was carried out by X-ray fluorescence using an Oxford Model ED2000 spectrometer. The excitation source was an X-ray tube with thin silver as the primary filter, operating at a tube voltage of 35 kV.

X-ray diffraction patterns were recorded using an X-ray diffractometer (Bruker AXS Model D8 Discover) with Ni-filtered Cu Kα (λ = 0.154 nm) radiation at a tube voltage of 40 kV and a tube current of 40 mA. The samples were scanned in a step mode at a scan rate of 1.5°/min from 2θ = 1–10°. The d_{001}-spacing was calculated on the basis of Bragg's equation ($\lambda = 2d\sin\theta$).

TEM observations were made on a TEM zero A H-7650 (Hitachi High-Technologies Co., Japan) operating at an accelerating voltage of 100 kV. The collected samples were dispersed in distilled water under sonication for 5 min. After that, one drop of dilute suspension of the samples was deposited on a copper grid and left for drying overnight. In another observation, ultra-thin sections, approximately

75 nm thick, were cryogenically cut with a diamond knife at a temperature of -110°C using a LEICA ULTRA CUT and were collected on copper grids.

SEM observations were performed with a JEOL model JSM-5200. The samples were fractured in a liquid nitrogen bath, adhered on brass stubs by using adhesive tape, and coated with gold under vacuum. All SEM digitized photographs were taken at an acceleration voltage of 15 keV with a magnification of 3500.

The volume electrical conductivity (σ_{dc}) was measured via the two-point probe technique using a Keithley 8009 Resistivity Test Fixture with a dc voltage from 1 to 100 V. The compression molded sheets were cut into a round edge shape six inches in diameter and placed in the Keithley 8009 test fixture. The voltage was applied across the sample, and the current was read by an electrometer. Then, the volume electrical conductivity was calculated via the following equations:

$$R = \frac{V}{I}, \tag{7.1}$$

$$\rho_v = \frac{22.9V}{tI}, \text{ and} \tag{7.2}$$

$$\sigma_{dc} = \frac{1}{\rho_v}, \tag{7.3}$$

where R is the resistance (Ω), V is the voltage (volts), I is the current (A), ρ_v is the volume resistivity (Ωcm), t is the sample thickness (cm), and σ_{dc} is the volume conductivity (Scm^{-1}).

Thermal stability studies were performed by using a Perkin-Elmer Pyris Diamond TG/DTA on samples weighing about 15–20 mg, at a heating rate of 10°C/min from 30°C to 600°C in a nitrogen atmosphere.

Hardness measurements were carried out with a Shore A durometer according to ASTM D-2240. Five different positions were measured and taken in an average. Tensile tests were performed on a Universal Testing Machine (LLOYD LR 100K) at a crosshead speed of 50 mm/min and a gauge length of 15 mm under room temperature according to ASTM D638M-91a. Five specimens were tested and taken in an average.

7.4 Results and Discussion

7.4.1 Synthesis of the Nanocomposites

On the basis of admicellar polymerization technique, there are four major steps taking place in an aqueous solution, which are admicelle formation, monomer adsolubilization, polymerization, and surfactant removal [9-11]. A main function of added anionic surfactant (SDS) is to form surfactant bilayers on the NR surface for the adsolubilization of all pyrrole monomers between those bilayers. Then, the upper layer is removed (as much as possible) after completing the polymerization in order to expose an ultrathin PPy film. As described by Bunsomsit et al. [9], the equilibrium SDS concentration after either pyrrole adsolubilization or adding an initiator is less than its critical micelle concentration (CMC), indicating that micelles are still not formed. As the pH is maintained at 3, pyrrole monomers are inevitably protonated, and it is suggested that protonated pyrrole orients its NH^+ to the palisade region (between the negatively charged head-groups of SDS), and with the hydrophobic moiety to the surfactant tail inside the bilayers. It turns out that an adsorption of protonated pyrrole on SDS also facilitates this orientation rather than the detachment of SDS from the NR surface into the solution. Considering the alignment of the protonated pyrrole to be thermodynamically favorable and stable, the highly concentrated pyrrole monomers at the solid–liquid interface will lead to the growth of PPy layer over the NR substrate after the polymerization. Similar observation was found by Funkhouser et al. [14] who stated that pyrrole, being a hydrophilic species, probably adsolubilizes in the head group region of the admicelle.

The electrochemical polymerization proceeds with a color change from a white solution to dark-grey followed by the deposition of the synthesized composites (NR/PPy or NR/PPy/MMT) at the anode electrode, and finally to black solution with the separation of the residual composite layer, which can be easily collected. Since no residual monomer is left over, this suggests that the pyrrole is completely polymerized. The electrochemical polymerization data of NR/PPy and a series of the nanocomposites are summarized in Table 7.1. Note that the polymerization rate (Table 7.1) is calculated from the initial slope of a plot between accumulated mass at the anode electrode and polymerization time (not shown here).

It can be clearly seen that the polymerization process is strongly influenced by the clay loadings; that is, the higher the clay content, the faster the polymerization reaction. Therefore, this suggests that there is a catalytic effect from the constituents, especially an oxidizing agent like Fe^{3+}, existing in the Na-MMT clay on the polymerization reaction. Previous studies [15, 16] have reported similar observations. The induction period and whole polymerization time of the synthesized polyaniline (PAN)–DBSA were greatly reduced in the presence of mica, talc, and organophilic clay. The authors demonstrated that some metallic ions such as Fe^{3+}, Fe^{2+}, Mg^{2+}, Ca^{2+}, etc., in mica, talc, and organophilic clay had a catalytic effect on the polymerization process, especially Fe^{3+} and Fe^{2+} ions. X-ray fluorescence spectra (Table 7.2) are employed here for determining the elemental contents of the MMT clay. As expected, the XRF data revealed that the MMT clay contains 1.39 wt% of Fe^{3+} ion. Comparing the 3–6 wt% and 0.7 wt% Fe^{3+} ion in mica and talc, respectively [15], it is undoubtedly that the 1.39 wt% Fe^{3+} ion present in the MMT clay is effective enough to accelerate/catalyze the polymerization process of pyrrole over the surface of the NR particles.

The FTIR spectra of pure PPy, NR/PPy, and the nanocomposites are shown in Fig. 7.1. Figure 7.1a shows a comparison of the FTIR spectra between pure PPy and NR/PPy composite. The bands at 1552, 1459, 1293, and 1050 cm^{-1}, corresponding to C=C stretching vibrations in the pyrrole ring, C-N stretching vibration, C-N in-plane deformation, and C-H in-plane deformation vibration, respectively, are the characteristic absorption peaks of the pure PPy sample [3, 17, 18]. For the NR/PPy composite, the bands related to NR at 2853–2960 (C-H stretching vibration), 1662 (C=C stretching vibration), 1448 and 1380 (C-H bending) cm^{-1}. and the bands related to PPy at 1310 (C-N in-plane deformation) and 1040 cm^{-1} (C-H in-plane deformation vibration) are evidenced. Also, the appearance of the band at 1090 cm^{-1} in NR/PPy points to the in-plane deformation vibration of $N^{+}H_2$ on protonated nitrogen [17]. This spectrum confirms the success of the electrolytic admicellar polymerization of PPy on NR particles. However, it is worthwhile to note that through admicellar polymerization, ultra-thin film PPy can be formed on the surface of NR particles, and thus there is a possibility that the bands at 1552 and 1459 cm^{-1} of PPy might not be detected. The content of residual SDS is less

compared to the contents of NR and PPy, and the peaks belonging to the SDS at 2800–3000 (C-H stretching vibration) and 1080 (stretching vibration of R-O-SO_3^-) cm^{-1} are not clearly observed [19], but are overlapped by the bands of NR and protonated PPy, respectively, as well.

The comparison of FTIR spectra between NR/PPy and the nanocomposites is presented in Fig. 7.1b. The bands associated with PPy remain present in those spectra, proving that NR particles are successfully coated with PPy despite the presence of the layered silicates. Owing to the chemical compositions of the MMT clay, its characteristic bands appear at 1040 (Si-O), 600 (Al-O), and 420 (Mg-O) cm^{-1}, according to the literature [20]. Based on Fig. 7.1b, the band at 1040 (Si-O) cm^{-1} is overlapped by the band of the C-H in-plane deformation vibration of PPy located at the same position. Nevertheless, the intensity of this band is much stronger in the case of the nanocomposites, indicating the existence of the layered silicates in the composites.

The most remarkable change after incorporation of the layered silicates is a shift of the band at 1090 cm^{-1} (in-plane deformation vibration of N^+H_2) of the unfilled NR/PPy sample towards lower wavenumber of the nanocomposites (*'red shift'*). This is initially ascribed to the possibility of having a slight interaction between positively charged PPy chains and negatively charged surfaces of the layered silicates, which might produce a short range ordering of the PPy chain along the clay platelet and promote the electrical conductivity. A similar observation has been reported by Omastová and co-workers [17] on PPy samples prepared in the presence of anionic surfactants. They stated that the interaction between anionic surfactants and PPy through ionic bonding possibly modifies the parameters of the conducting network created by the PPy chains, and the chain regularity; consequently, a small red shift of the bands at 1552 cm^{-1} (C-C stretching vibration of the ring) is observed, which contributes to the enhancement in electrical conductivity. To test our hypothesis, electrical conductivity was investigated and is discussed later in the conductivity part.

7.4.2 Dispersion of the Layered Silicates and Morphology of the Nanocomposites

Considering the fact that pristine clay possesses hydrophilicity, the extent of separation between layer planes through adsorption of water is typically dependent on type of swelling, type of clay, and the cations that counterbalance the negatively charged siloxane faces, as stated by Bandi et al. [21]. Most of the time, MMT with Na^+ or Li^+ as the interlayer monovalent cations provides a quite good dispersion in water (strong hydration), enabling the further penetration of relatively large-sized molecules into the intergallery [21, 22]. Due to the negatively charged surface of layered silicates, it is believed that they might move towards the anode electrode together with pyrrole and NR particles [23] through this electrochemical polymerization and are completely encapsulated within the PPy matrix, which is a polar material. Thus, XRD and TEM observations were carried out to understand the proposed mechanism. Figure 7.2 displays the XRD patterns of Na-MMT clay and the series of nanocomposites.

The Na-MMT clay shows a diffraction peak at 2θ equal to 6.10°, corresponding to a d_{001}-spacing of 1.41 nm. Interestingly, no diffraction peak is observed in the range from 2 to 10° for the nanocomposites, indicating the possibility of having fully delaminated layered silicates dispersed in the PPy matrix. However, at a considerably high clay loading, e.g. 7 phr, poorer dispersion and stacking of the clay layers appear, and more importantly, when the MMT loading exceeds 7 phr, self-aggregation between the layered silicates and NR particles occurs, leading to the formation of an aggregated bulkier form, which will segregate away from the system; thus it is not suitable for preparing the nanocomposites. In other words, the MMT is now acting as a flocculating agent that causes the agglomeration of NR latex particles. As a result, we chose 7 phr to be the upper limit of MMT loading for this research.

Figure 7.3a shows a typical TEM photograph taken from a 1 wt% clay aqueous suspension. Herein, clay particles are fully swollen and partially peeled off into either individual layers or expanded silicate layers due to the applied shear force. This result is in accordance with that of Wu [22]. TEM photographs of NR particles, unfilled NR/PPy, and the nanocomposites are also displayed in Fig. 7.3. Note that

TEM analysis provides clear evidence for the dispersion of layered silicates in the polymer matrix. The dark particle and dark lines represent the NR particle and the layered silicates, respectively; whereas the pale edge represents the tiny conductive polymer nodules (PPy). As shown in Fig. 7.3c, a typically smooth and uniform PPy overlayer is formed on the swollen surface of the NR particle, which truly confirms the NR/PPy core–shell structure.

With the incorporation of layered silicates, one can notice that a smooth and uniform core–shell structure, as observed in Fig. 7.3c, is no longer attained; that is, there is a distortion in the uniform spherical shape of the coating layer owing to the long lateral dimension of the layered silicates. The existence of layered silicates in the PPy matrix is obviously seen for the 7 phr-filled composite. Individual silicate layers, along with some layered stacks (up to 50 nm in thickness), are qualitatively identified, as revealed in Fig. 7.3g. On the contrary, after compression molding, those tactoids tend to be noticeably further delaminated into less than 10 nm in thickness with random orientations, as shown in Fig. 7.3h, and thus it is ascertained that an exfoliated structure is achieved. Those images (Fig. 7.3c–h) also reveal the good compatibility between the clay and swollen rubber, as seen by the uniform dispersion of the clay platelets. Based on the XRD patterns and TEM photographs, we certainly conclude that the layered silicates are successfully incorporated into a NR/PPy core–shell structure during the electrochemical polymerization. To get more insight into the structure of electropolymerized nanocomposites, we herein also illustrate the coating mechanism of the NR/PPy core–shell structure comprising layered silicates during electropolymerization, as schematically depicted in Fig. 7.4.

SEM micrographs of the NR/PPy and the series of nanocomposites are displayed in Fig. 7.5. The admicelled rubber (Fig. 7.5a) exhibits a nice *'cauliflower-like appearance'* with closely-packed layers of tiny PPy nodules over the surface of the NR core particles, corresponding to the previous work [1, 11]. Again, this correlates well with the existence of the core–shell structure. Generally, as a surfactant is added to enhance the dispersion of rubber in water, NR latex particle can be swollen to a slight distance, as seen from TEM images (not shown here). The swollen boundary of the NR particle will be a preferential site for tiny PPy nodules to

reside in during the admicellar polymerization. Finally, the NR core is completely surrounded by the PPy shell. However, some of the PPy nodules can penetrate into the swollen boundary of the NR particle, which means that the exterior shell is now composed of not only PPy nodules but also of some of the swollen boundary of the NR particle. As water evaporates during the drying of the composite, the swollen boundary located outside the core–shell structure possibly acts as a binder, consolidating each core–shell particle, producing a continuous morphology, as observed in Fig. 7.5a. In addition, no obvious phase separation between PPy and NR is evidenced, signifying a high level of dispersability of the NR particles and the PPy nodules. Considering the effect of layered silicates, it is noticeable that they greatly influence the morphology of the synthesized nanocomposites. Figures 7.5c and 7.5d reveal the presence of some micrometer-sized hollow spheres in the nanocomposites containing 3 and 5 phr loading, respectively. This originates from the brittleness of the layered silicates that causes the exclusion of some NR core particles during breakage under liquid nitrogen temperature. Figure 7.5e indicates that the 7 phr loading of layered silicates causes the morphology of electropolymerized nanocomposites to be more compact, rougher, and denser compared to unfilled NR/PPy. Besides, all of the plate-like silicate layers are covered with PPy, ascribing to the growth and assembly of the PPy overlayer on ordered templates provided by the clay platelets, which promotes the short range ordering of the PPy chain. This could be an indirect evidence for the enhancement in electrical conductivity because Liu et al. [5] proved that a denser and more compact morphology of the electropolymerized PPy/clay composite provided an improvement in conductivity by 24 times compared to pure PPy. In brief, the SEM micrographs (Fig. 7.5) are in good agreement with the above-mentioned XRD and TEM studies, i.e. the layered silicates are successfully incorporated into the NR/PPy core–shell structure.

7.4.3 Electrical Conductivity

As we know, NR is an insulating material having an electrical conductivity of 7.18×10^{-15} Scm^{-1}, whereas $LiClO_4$-doped PPy prepared by electropolymerization shows an electrical conductivity of 26.4 Scm^{-1} [5]. In this study, admicelled rubber exhibits an electrical conductivity of 3.1×10^{-6} Scm^{-1},

which is about nine orders of magnitude higher than that of neat NR. This explains that the connection of each PPy-coated NR particle provides a smooth pathway for effective charge transportation along the PPy chains without any interference from the underlying electrically insulating core NR; as a consequence, the conductivity of NR is improved. Similar observations have been found in other studies of polymer-based composites, e.g. micrometer-sized PPy-coated PS latexes [8] and PPy-coated acetylamine-modified silica particles [24].

It was known that the insulating layered silicates may lower the electrical conductivity of the nanocomposites; however, in this study, they exhibit extraordinary behavior. The electrical conductivity of the nanocomposites is displayed in Fig. 7.6. Interestingly, the electrical conductivity of the nanocomposites is about 19–32 times higher than that of unfilled NR/PPy. The improvement in electrical conductivity with the addition of clay layers is relatively high in comparison to the studies of Liu and Ger (~ 24 times) [5] and Jia et al. (~ 2–3 times) [16]. This is explained by the following:

(i) As described earlier in the FTIR spectra, there is a small red shift of the band at 1090 cm^{-1}(in-plane deformation vibration of $N^{+}H_2$), indicating a slight interaction between the positively charged PPy chains and the negatively charged surfaces of the layered silicates. It is suggested that, through this electrostatic interaction, the structural disorder of the PPy chain tends to change into an extended chain conformation, facilitating the electron hopping along the chain; thus the electrical conductivity is enhanced. As shown in the literature [16, 25], the conductivity of the chemically synthesized PAN/clay nanocomposite was increased due to the confined environment of the PAN chain in the clay gallery producing the extended chain conformation with high conjugation.

(ii) Based on SEM micrographs, the morphologies of the electropolymerized nanocomposites are much denser, rougher, and more compact especially for the 7 phr-filled composite; as a result, the interchain electron hopping takes place more easily [5], and the electrical conductivity is improved.

Accordingly, it is worthwhile to note that Na-MMT clay can be a helpful inorganic material to promote the electrical conductivity of the unfilled NR/PPy through altering the coating morphology and providing a short range

ordering of the PPy chain along the clay surface, which facilitates the free motion of charge carriers.

7.4.4 Thermal Stability Study

Figure 7.7 shows the thermogravimetric curves (TGA) for pure NR, PPy, and NR/PPy composite. It can be seen from the TGA curve that the NR sample is fully decomposed, while the PPy shows a residual content of 66.6 wt% at 600°C. The onset and main decomposition temperatures of NR are located at 351.6 and 373.6°C, respectively. As a comparison, PPy shows two stages of weight loss. The first weight loss of about 5 wt% at temperatures up to 100°C is due to the loss of residual moisture in the PPy, which normally is a hygroscopic material [17]. The second weight loss of about 28 wt% in the temperature range from 200–400°C is assigned to the decomposition of PPy itself [5, 6]. In addition, the onset and main decomposition temperatures of PPy are 204.9 and 260.3°C, respectively.

As for admicelled rubber, a two-step weight loss process is clearly observed. The first weight loss (10.5 wt%), ranging from 160 to 300°C, contributes to the decomposition of PPy, some surfactant, and the acid dopant (HCl) [26]. The second weight loss can be further separated into two stages. The first stage (52.6 wt%), ranging from 300 to 400°C, is assigned to the decomposition of the swollen NR, which is more exposed to the heating compared to the NR core; whereas the second stage (17.7 wt%), ranging from 400 to 480°C, is assigned to the decomposition of the NR core. Thus, the total weight loss in the temperature range 300–480°C is about 70.3 wt%, which is approximately the weight percentage of NR (major component). The residual content after 500°C is about 19 wt%, which is relatively high with regard to the calculated residual content of 100 mM PPy (~10 wt%), implying the incomplete decomposition of the NR core. In order to effectively determine the thermal stability of the composite, the derivative curve (DTG) is investigated as well. Figures 7.8a and 7.8b show the TGA and corresponding DTG curves of unfilled NR/PPy and the series of nanocomposites, respectively. The details of the decomposition processes for all systems are summarized in Table 7.3. It is evident that the main decomposition temperature (T_{d2}) of admicelled rubber reduces by about 3.4°C with respect to pure NR. Again, this is ascribed to the

decomposition of the swollen NR with no thermoshielding effect by the PPy shell. On the other hand, the occurrence of a shoulder in the temperature ranging from 400 to 480°C with slower decomposition rate, compared to that of the main peak, demonstrates a unique characteristic of admicelled material, in which the PPy shell performs as a thermoprotecting layer, delaying the decomposition of the NR core. For that reason, the NR core may not be fully decomposed, and the residual content of the admicelled rubber is somewhat high relative to that of 100 mM PPy itself.

Obviously, the TGA and DTG curves of the nanocomposites are similar to those of the unfilled NR/PPy. As summarized in Table 7.3, there is a shift in $T_{d,1}$ towards higher temperature for 1, 3, and 5 phr-filled composites, which confirms an improvement in thermal stability for PPy by the layered silicates. This is expected because, as stated at the beginning, we find that there is a slight electrostatic interaction between the positively charged PPy chains with the negatively charged face of the layered silicates, which can further restrict the segmental mobility of the PPy chains and delay them from undergoing thermal decomposition [5, 6]. The shielding effect by these layered silicates was found in the case of PAN/clay nanocomposites as well [16, 26-28]. In the case of the 7 phr-filled composite, the DTG curve is almost constant as the temperature increases up to 300°C, and the $T_{d,1}$ is no longer observed. This also indicates the barrier effect imparted by clay layers that rather causes PPy to be decomposed at higher temperature.

It is interesting that the thermal behavior of the NR component is strongly influenced by the layered silicates. This is documented by the following evidences. (i) Based on the TGA curves, the weight losses corresponding to the swollen NR (300–390°C) and NR core (390–500°C) initially decrease, then increase with an increase in MMT content, and finally approach a maximum at a 7 phr loading. It should be mentioned here that the clay layers exhibit two effects on the NR at the same time; those are, the thermoshielding behavior (at lower content) and the thermooxidative behavior (at higher content). Additionally, due to this maximum weight loss at a 7 phr loading, it can be considered that the PPy itself decomposes simultaneously with the swollen NR in the temperature range 300–390°C. (ii) Considering the residual weights of the nanocomposites, the 3 phr-filled composite

shows the highest residual weight—that is, the highest content of residual NR core—whereas the 7 phr-filled composite shows the lowest value. This is also explained by the above mentioned behavior of the clay layers. (iii) Based on the DTG curves, the decomposition rates at the main peak ($T_{d,2}$) and at the shoulder ranging from 390 to 500°C are retarded for 1, 3, and 5 phr-filled composites with respect to that of unfilled NR/PPy. The decrease in decomposition rate at lower clay content describes the screening effect offered by the clay layers. Besides, the $T_{d,2}$ of 1, 3, and 5 phr-filled composites are remarkably less than that of the unfilled NR/PPy and pure NR. A lowering in thermal stability of swollen NR upon the incorporation of clay layers is ascribed to the Fe^{3+} present in the octahedral sheets of Na-MMT. It is known that transition metal cations (e.g. Fe^{3+}) at planar surfaces of smectite clay can act as oxidizing agents, and their oxidizing ability becomes more pronounced at high temperature [29]. Our previous work [30] has reported an acceleration in the thermal decomposition of NR vulcanizate by the Fe^{3+} present at the octahedral sheet of smectite clay. Acceleration in thermooxidative aging of the rubber masterbatch was also evidenced by those metals present in the clay [31]. Morlat et al. [32] proposed that the ferric ion in Na-MMT catalyzed the decomposition of polypropylene (PP), as indicated by a decrease in the induction period of the photo-oxidation reaction of the PP/MMT nanocomposite. For the 7 phr-filled composite, as the PPy component completely decomposes and forms the thermoprotecting carbonaceous layer around the NR core, one can observe a broad DTG curve with slow decomposition rate and a shift in $T_{d,2}$ towards higher temperature, as seen in Fig. 8b. However, the maximum weight loss of the NR component is mainly a result of a higher amount of added MMT—that is, higher oxidizing sites (Fe^{3+}) present in the system, compared to the others.

The weight percentage of NR/PPy and its nanocomposites remaining at 550°C is presented in Table 7.4 along with the residual content of the NR core, the PPy and the MMT. It is found that the weight percentage of the residual NR core does not show any regular trend, while that of the residual PPy is comparable for all systems except for the 7 phr-filled composite. As explained earlier, an incomplete decomposition of the NR core points to the occurrence of a thermoprotecting carbonaceous layer through the decomposition of PPy, and 3 phr-filled composite

shows the highest residue at 550°C; that is, the highest content of residual NR core. All these results show that a 3 phr loading should be the optimum for improving the thermal stability of the nanocomposites, as evidenced by a shifting in $T_{d,1}$ towards higher value, the slower decomposition rate at $T_{d,2}$, and the highest residual content of the NR core, compared to the others.

Again, we prove that the incorporation of these inorganic species, e.g. MMT clay, into organic matrices does not always improve the thermal stability of organic polymer matrices, especially when the clay layers are constituted of Fe^{3+} in their crystalline structure, and the matrix is unsaturated polymer.

7.4.5 Mechanical Properties

Comparative studies of the mechanical properties of pure NR, NR/PPy, and the nanocomposites are shown in Table 7.5. The unfilled NR/PPy showed 102%, 100%, 160%, and 17% improvements on Shore A hardness, stress at 100% elongation, initial modulus, and tensile strength, respectively, in comparison to the values obtained for pure NR. However, the elongation at break of the unfilled NR/PPy is less than the pure NR. The improvement in those properties is ascribed to the hard and brittle behavior of the PPy component, which performs as an effective reinforcing filler for the NR component.

The mechanical performance of the nanocomposites is clearly dependent on the clay loading; that is, the mechanical properties increase effectively with increasing content of clay from 3 to 7 phr and reach a maximum value at 7 phr loading, as we expected. Shore A hardness of the nanocomposites containing 5 and 7 phr of clay increases by 28 and 31%, respectively, in comparison to that of the unfilled NR/PPy. The initial modulus and tensile strength of the 7 phr-filled composite are about 4 and 2 times greater than unfilled NR/PPy, respectively. The elongation at break of the nanocomposites also increases considerably from 119 to 414% with increasing clay content up to 7 phr. On the other hand, all of the nanocomposites exhibit almost the same numerical value of 100% tensile stress. From the above testing results, this reinforcing effect is explained in terms of the uniform dispersion of clay layers in the polymer matrix at the nano level, as illustrated earlier on the XRD patterns and TEM observations, and the planar

orientation of the clay layers [22, 33]. The nanometer dispersion of the clay layers generally facilitates the interfacial interaction between the clay layers and the polymer matrix, further providing an efficient capability to withstand the built-up stress and restricting the mobilization of the polymer chains.

7.5 Conclusions

So far, many attempts have been made to improve the electrical conductivity of pure NR. In the current study, we explored the first exfoliated organic–inorganic composites consisting of NR, PPy, and Na-MMT that were successfully prepared by electrolytic admicellar polymerization, as confirmed from FTIR spectra. The polymerization process was dramatically accelerated by Fe^{3+} in the layered silicates. XRD patterns strongly indicated the incorporation of layered silicates into the NR/PPy core–shell structure, fully delaminating into individual platelets. As depicted in TEM and SEM micrographs, the layered silicates caused a distortion in the uniform covering of PPy over the NR particle. In addition, owing to the ordered template provided by the clay platelets, the growth and assembly of the PPy overlayer on the clay surface were subsequently observed, resulting in a more compact and denser morphology of the nanocomposites, especially at 7 phr loading. Compared to the unfilled NR/PPy, the nanocomposites exhibited a significant improvement in electrical conductivity, about 19–32 times. TGA studies showed that the layered silicates had a delay effect on the thermal stability for the PPy component, while greatly accelerating the thermal decomposition of the NR component. Additionally, the best thermal performance can be achieved at a 3 phr loading of MMT. The Shore A hardness, initial modulus, tensile strength, and elongation at break of the nanocomposites were remarkably improved as compared to the unfilled NR/PPy.

7.6 Acknowledgements

The authors are grateful to the Thailand Research Fund through the Royal Golden Jubilee Ph.D. Program (PHD/0088/2549) for providing financial support.

The authors also want to acknowledge Hitachi High-Technologies Corporation, Mr. Wonchalerm Rungswang, and Dr. Suwabun Chirachanchai for performing the morphological observation via TEM zero A H-765.

7.7 References

[1] Yigit, S.; Hacaloglu, J.; Akbulut, U.; Toppare, L. Synthetic Metals 1996, 79, 11.

[2] Yigit, S.; Hacaloglu, J.; Akbulut, U.; Toppare, L. Synthetic Metals 1997, 84, 205.

[3] Kim, J.W.; Liu, F.; Choi, H.J.; Hong, S.H.; Joo, J. Polymer 2002, 44, 289.

[4] Sadki, S.; Schottland, P.; Brodie, N.; Sabouraud, G. Chem. Soc. Rev. 2000, 29, 283.

[5] Liu, Y.C.; Ger, M.D. Chemical Physics Letters 2002, 362, 491.

[6] Hong, S.H.; Kim, B.H.; Joo, J.; Kim, J.W.; Choi, H.J. Current Applied Physics 2001, 1, 447.

[7] SinhaRay, S.; Biswas, M. Materials Research Bulletin 1999, 34, 1187.

[8] Lascelles, S.F.; Armes, S.P. J. Mater. Chem. 1997, 7, 1339.

[9] Bunsomsit, K.; Magaraphan, R.; O'Rear, E.A.; Grady, B.P. Colloid Polym Sci 2002, 280, 509.

[10] Genetti, W.B.; Yuan, W.L.; Grady, B.P.; O'Rear, E.A.; Lai, C.L. Journal of Materials Science 1998, 33, 3085.

[11] Chirasakulkarun, A. in The Petroleum and Petrochemical College; Chulalongkorn University, Bangkok: 2008.

[12] Li, Y.; Cheng, X.Y.; Leung, M.Y.; Tsang, J.; Tao, X.M.; Yuen, M.C.W. Synthetic Metals 2005, 155, 89.

[13] Kim, H.K.; Kim, M.S.; Chun, S.Y.; Park, Y.H.; Jeon, B.S.; Lee, J.Y.; Hong, Y.K.; Joo, J.S.; Kim, S.H. Mol. Cryst. Liq. Cryst. 2003, 405, 161.

[14] Funkhouser, G.P.; Arévalo, M.P.; Glatzhofer, D.T.; O'Rear, E.A. Langmuir 1995, 11, 1443.

[15] Jia, W.; Segal, E.; Narkis, M.; Siegmann, A. Polym. Adv. Technol. 2002, 13, 16.

[16] Jia, W.; Segal, E.; Kornemandel, D.; Lamhot, Y.; Narkis, M.; Siegmann, A. Synthetic Metals 2002, 128 , 115.

[17] Omastová, M.; Trchová, M.; Kovářová, J.; Stejskal, J. Synthetic Metals 2003, 138, 447.

[18] Xing, S.; Zhao, G. Materials Letters 2007, 61, 2040.

[19] Rungruang, P.; Grady, B.P.; Supaphol, P. Colloids and Surfaces A: Physicochem. Eng. Aspects 2006, 275, 114.

[20] Yeh, J.M.; Liou, S.J.; Lai, C.Y.; Wu, P.C. Chem. Mater. 2001, 13, 1131.

[21] Bandi, S.A. Unpublished Ph.D. Dissertation, Case Western Reserve University, Cleveland, Ohio.

[22] Wu, Y.P.; Wang, Y.Q.; Zhang, H.F.; Wang, Y.Z.; Yu, D.S.; Zhang, L.Q.; Yang, J. Composites Science and Technology 2005, 65, 1195.

[23] Talib, Z.A.; Daud, W.M.; Khalid, K.B.; Mat-Yunus, W.M.; Mansor, A.R. IEEE Transactions on Dielectrics and Electrical Insulation 1998, 5, 195.

[24] Yang, X.; Dai, T.; Lu, Y. Polymer 2006, 47, 441.

[25] Wu, Q.; Xue, Z.; Qi, Z.; Wang, F. Polymer 2000, 41, 2029.

[26] Lee, D.; Char, K. Polymer Degradation and Stability 2002, 75, 555.

[27] Kim, B.H.; Jung, J.H.; Hong, S.H.; Joo, J. Macromolecules 2002, 35, 1419.

[28] Yoshimoto, S.; Ohashi, F.; Ohnishi, Y.; Nonami, T. Synthetic Metals 2004, 145, 265.

[29] Theng, B.K.G. Clays and Clay Minerals 1971, 19, 383.

[30] Pojanavaraphan, T.; Magaraphan, R. Eur Polym J 2008, 44, 1968.

[31] Chen, M.; AO, N.J.; Chen, Y.; Yu, H.P.; Qian, H.L.; Wang, C.; Zhou, H.L.; Qu, J.L.; Guo, C.K. J Appl Polym Sci 2001, 82, 338.

[32] Morlat, S.; Mailhot, B.; Gonzalez, D.; Gardette, J.L. Chem. Mater. 2004, 16, 377.

[33] Wu, Y.P.; Jia, Q.X.; Yu, D.S.; Zhang, L.Q. J Appl Polym Sci 2003, 89, 3855.

Table 7.1 Electrochemical polymerization data of NR/PPy and a series of the nanocomposites

System	Polymerization time [hr]	Rate of polymerization [g/hr]
NR/PPY	27	1.03
NR/PPy/1 MMT	24	0.84
NR/PPy/3 MMT	14	1.33
NR/PPy/5 MMT	12	1.68
NR/PPy/7 MMT	12	1.87

Table 7.2 Elemental analysis of Na-MMT

Al	Si	S	K	Ca	Ti	Fe	Cu	Zn	Sr	Y	Zr
1.22[a]	7.27[a]	1286[b]	675[b]	0.39[a]	1165[b]	1.39[a]	62[b]	53[b]	59[b]	10[b]	45[b]

[a] wt%, [b] ppm.

Table 7.3 Summary of the decomposition processes for unfilled NR/PPy and the nanocomposites

System	Temperature range [°C]	Peak decomposition temperature [°C]	% weight loss
NR/PPy	160-300	243.19*	10.5
	300-400	370.20**	52.6
	400-480	-	17.7
NR/PPy/1MMT	160-300	243.70*	11.8
	300-390	359.03**	48.8
	390-500	-	18.3
NR/PPy/3MMT	160-300	244.62*	16.0
	300-390	361.98**	27.6
	390-500	-	15.8
NR/PPy/5MMT	160-300	247.07*	13.9
	300-390	362.00**	39.6
	390-500	-	12.3
NR/PPy/7MMT	160-300	-	6.9
	300-400	380.0**	41.8
	400-500	-	39.5

* $T_{d,1}$ (peak decomposition temperature with regard to the first weight loss).

** $T_{d,2}$ (peak decomposition temperature with regard to the second weight loss).

Table 7.4 Weight percentage of NR/PPy and its nanocomposites remaining at 550°C

System	Residual NR core [%]	Residual PPy [%]	Weight of MMT[a] [%]	Total residue at 550°C [%]
NR/PPy	10.29	9.31	-	19.6
NR/PPy/1MMT	8.46	9.21	1.03	18.7
NR/PPy/3MMT	24.43	9.03	3.04	36.5
NR/PPy/5MMT	17.29	8.85	4.96	31.1
NR/PPy/7MMT	1.75	-	6.81	8.56

[a] calculated from the feed composition.

Table 7.5 Mechanical properties of pure NR, NR/PPy, and the series of nanocomposites

System	Shore A hardness	Stress at 100 % elongation [MPa]	Initial modulus [MPa]	Tensile strength [MPa]	Elongation at break [%]
NR	22.5	0.3	0.5	0.6	829
NR/PPy	45.4	0.6	1.3	0.7	119
NR/PPy/1MMT	46.0	0.6	1.3	0.7	156
NR/PPy/3MMT	50.0	0.5	1.5	0.8	283
NR/PPy/5MMT	58.0	0.5	2.3	0.9	410
NR/PPy/7MMT	59.3	0.7	5.0	1.3	414

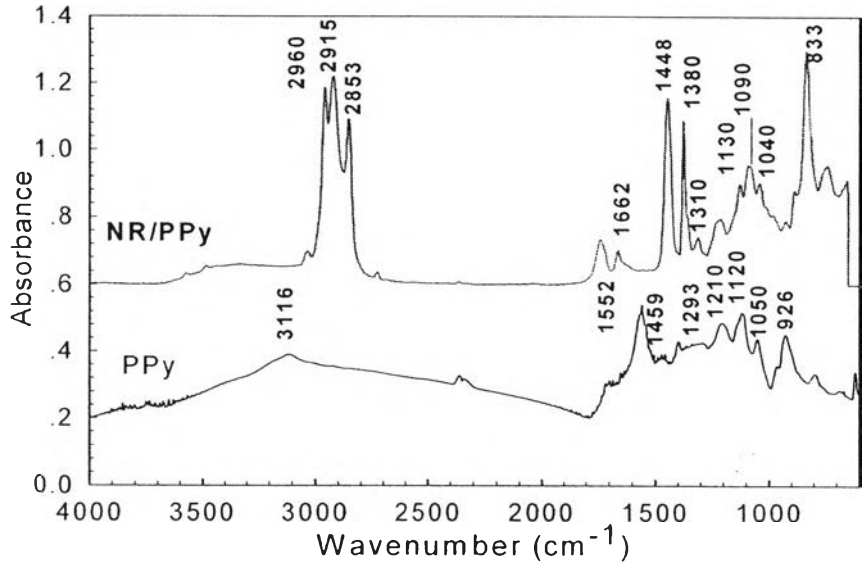

(a)

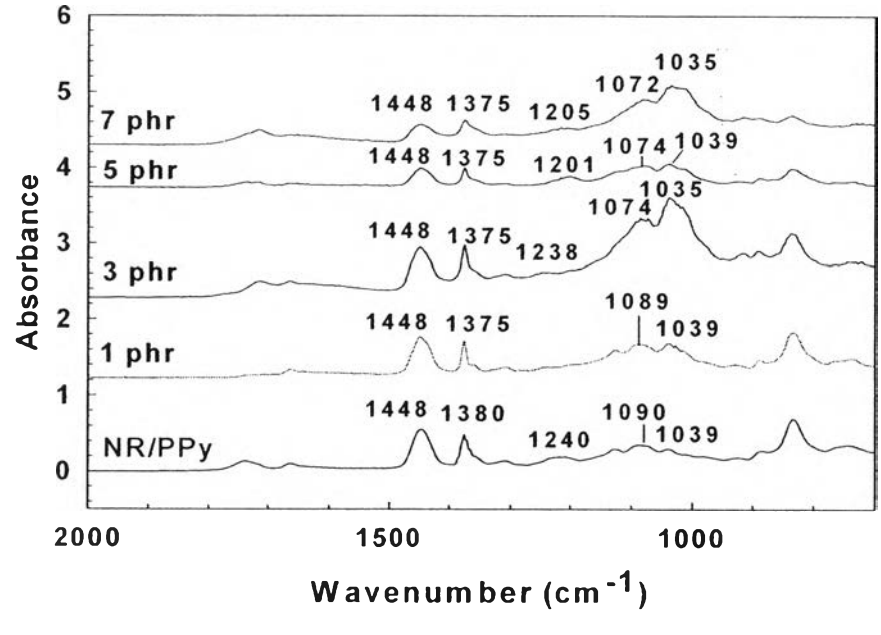

(b)

Figure 7.1 FTIR spectra of (a) pure PPy and NR/PPy; and (b) NR/PPy and the nanocomposites.

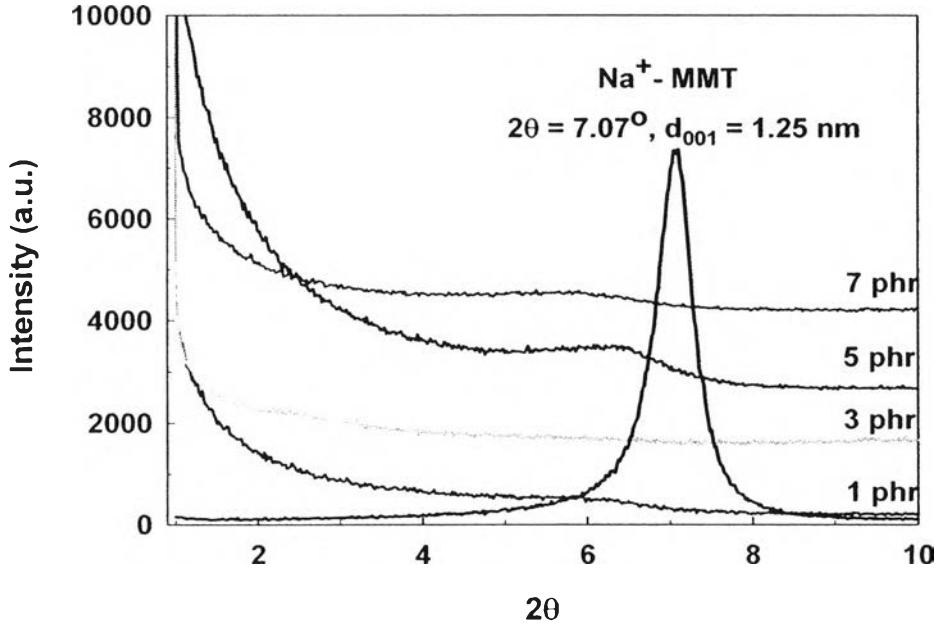

Figure 7.2 XRD patterns of Na-MMT and the series of nanocomposites.

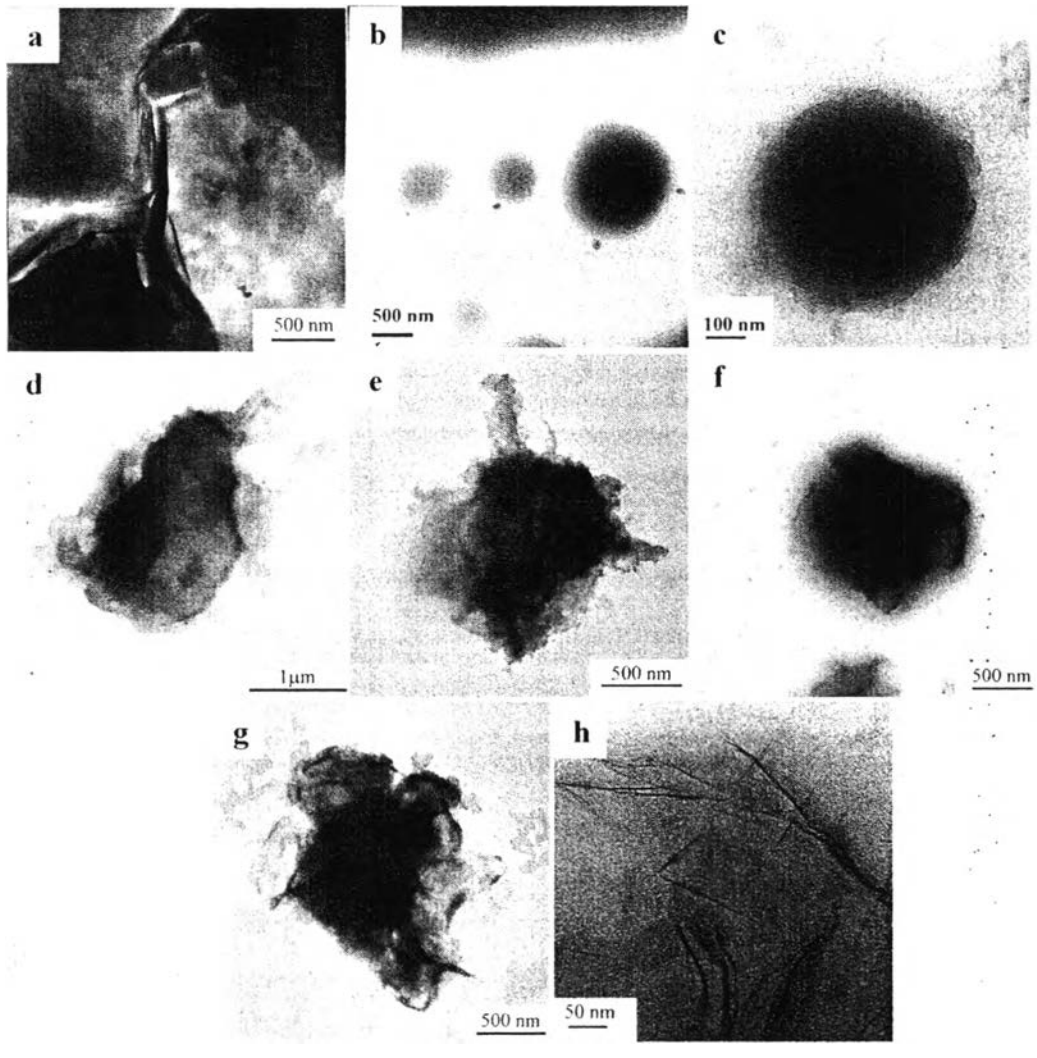

Figure 7.3 TEM photographs of (a) a 1 wt% clay suspension; (b) NR particles; (c) NR/PPy; and the nanocomposites containing (d) 1 phr; (e) 3 phr; (f) 5 phr; (g) 7 phr-MMT loading; and, (h) an ultrathin section of 7 phr-MMT loading.

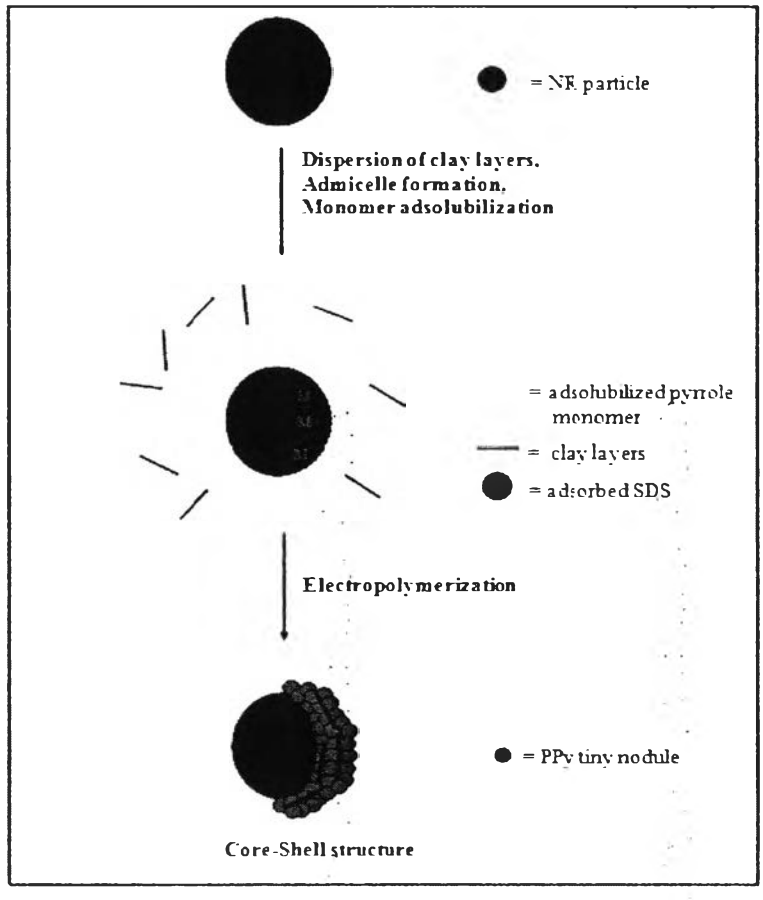

Figure 7.4 Schematic of the structure of electropolymerized nanocomposites.

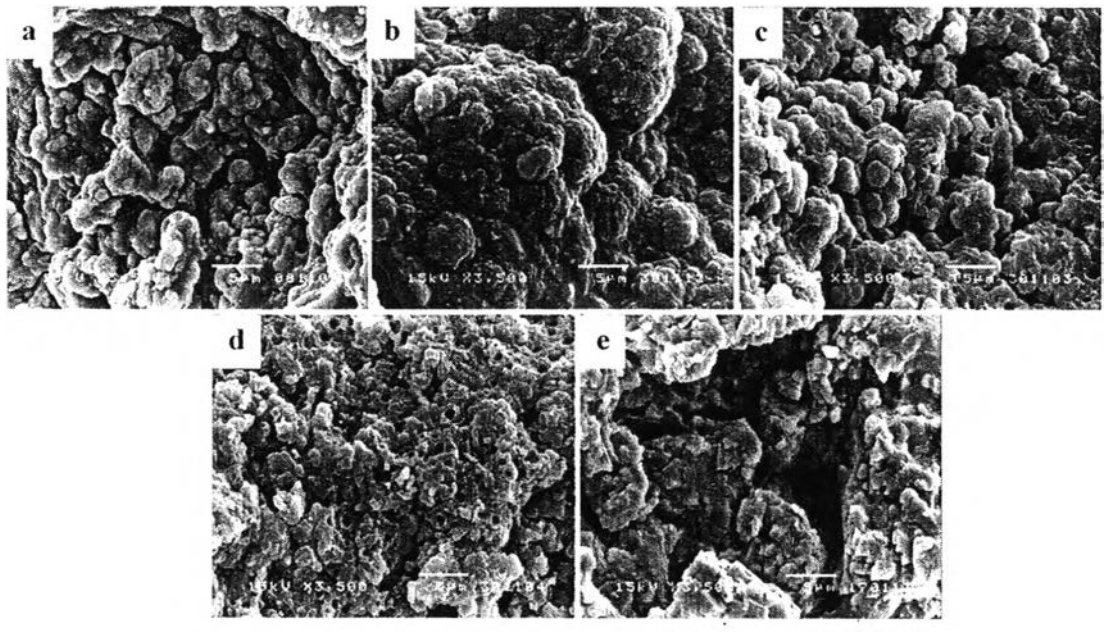

Figure 7.5 SEM micrographs of (a) NR/PPy; and the nanocomposites containing (b) 1 phr; (c) 3 phr; (d) 5 phr; and, (e) 7 phr-MMT loading at the same magnification (×3500).

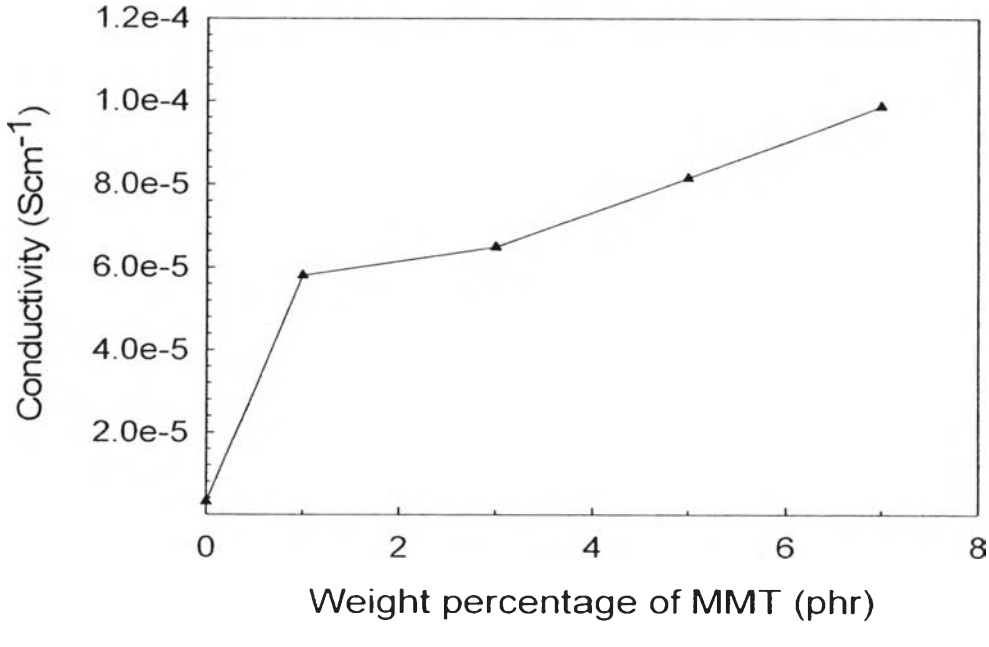

Figure 7.6 Electrical conductivity of NR/PPy and the series of nanocomposites.

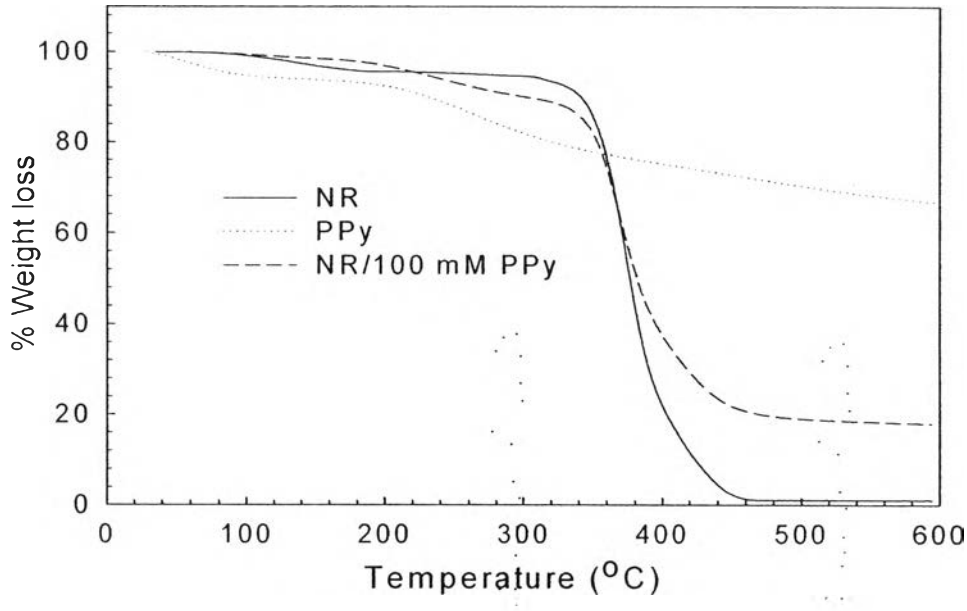

Figure 7.7 TGA curves of pure NR, PPy, and NR/PPy composite.

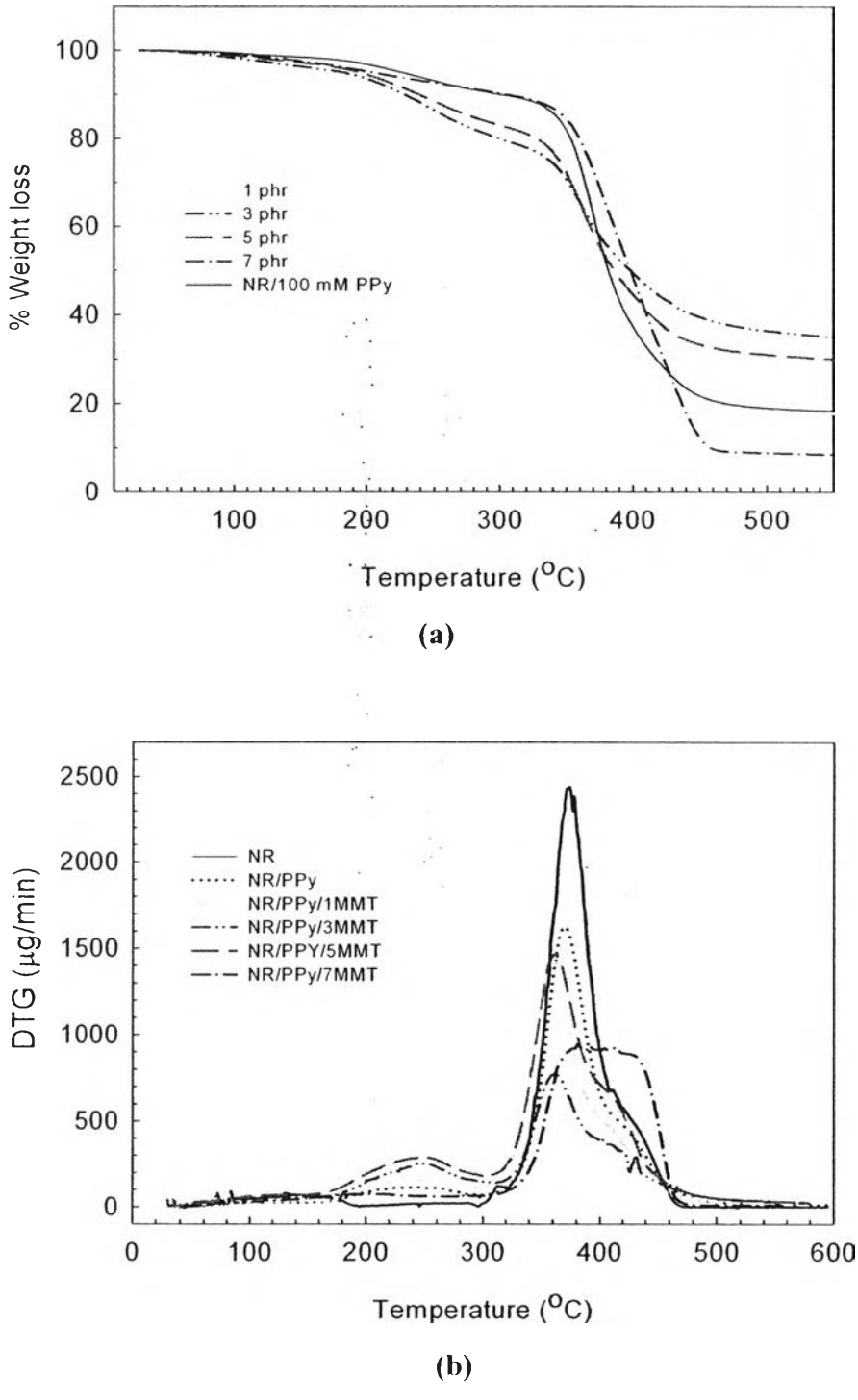

Figure 7.8 (a) TGA curves: and, (b) DTG curves of pure NR, NR/PPy and the series of nanocomposites.